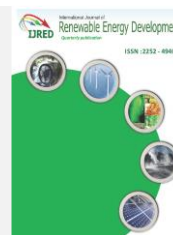




Contents list available at IJRED website

International Journal of Renewable Energy Development

Journal homepage: <https://ijred.undip.ac.id>



Research Article

Development of BiOBr/TiO₂ nanotubes electrode for conversion of nitrogen to ammonia in a tandem photoelectrochemical cell under visible light

Prita Amelia¹ and Jarnuzi Gunlazuardi*²

Department of Chemistry, Faculty of Mathematics and Natural Sciences, University of Indonesia, Indonesia

Abstract. Ammonia (NH₃) is one of the important chemicals for human life. The demand for ammonia is expected to increase every year. Conventionally, the fixation process of N₂ to produce NH₃ in the industrial sector is carried out through the Haber–Bosch process, which requires extreme temperature and pressure conditions that consume a high amount of energy and emit a considerable amount of CO₂. Therefore, it is necessary to develop alternative technology to produce ammonia using environmentally friendly methods. Many studies have developed the photo-electrochemical conversion of nitrogen to ammonia in the presence of semiconductor materials, but the resulting efficiency is still not as expected. In this research, the development of the tandem system of Dye-Sensitized Solar Cell - Photoelectrochemistry (DSSC - PEC) was carried out for the conversion of nitrogen to ammonia. The DSSC cell was prepared using N719/TiO₂ nanotubes as photoanode, Pt/FTO as cathode, and electrolyte I⁻/I₃⁻. The DSSC efficiency produced in this research was 1.49%. PEC cell at the cathode and anode were prepared using BiOBr/TiO₂ nanotubes synthesized by the SILAR (Successive Ionic Layer Adsorption and Reaction) method. The resulting ammonia levels were analyzed using the phenate method. In this study, ammonia levels were obtained at 0.1272 μmol for 6 hours of irradiation with an SCC (Solar to Chemical Conversion) percentage of 0.0021%.

Keywords: ammonia, BiOBr/TiO₂ nanotubes, DSSC, nitrogen fixation, photo-electrochemistry



@ The author(s). Published by CBIORE. This is an open access article under the CC BY-SA license (<http://creativecommons.org/licenses/by-sa/4.0/>).

Received: 29th Dec 2022; Revised: 26th March 2023; Accepted: 27th May 2023; Available online: 23rd June 2023

1. Introduction

Ammonia (NH₃) has a significant role in human life, including in industry and agriculture (Lan *et al.*, 2021). Ammonia is used as the main raw material in a variety of chemical products, such as fertilizers, nitric acid, and freezing agents (Feng *et al.*, 2021). In addition, NH₃ is an essential material for hydrogen storage with a high-energy hydrogen layer and is environmentally friendly. The global output of ammonia is about 15 billion tons per year (Huang *et al.*, 2021).

One important source of ammonia is the nitrogen (N₂) atmosphere (Cao *et al.* 2018). Although about 78% of the Earth's atmosphere contains nitrogen, most organisms find its molecular form unusable due to the non-polar covalent triple bonds of N≡N. This bond is highly resistant to dissociation and has a high ionization energy and negative electron affinity. Traditionally, the industrial fixation of N₂ to NH₃ was carried out via the Haber–Bosch process, which requires extreme conditions (400–600°C, 20–40 MPa) in the presence of an iron-based catalyst to overcome the kinetic limitations (Wang *et al.*, 2022). This process involves about 2% of the world's energy supply and emits 2.3 tons of CO₂ annually. In addition, the hydrogen gas used to synthesize NH₃ is mainly produced from the reformation of methane vapor, which requires about 3–5 % of the world's annual natural gas production and emits large

amounts of CO₂ (Li *et al.*, 2015). Given the shortage of fossil fuels and global climate change, a fixation process of nitrogen that requires less energy consumption is required for long-term goals. The catalytic process that produces NH₃ from N₂ at room temperature and atmospheric pressure is a promising method for the sustainable, safe, and clean synthesis of NH₃ (Olabi *et al.*, 2023).

The photo-electrocatalytic reaction to convert N₂ to NH₃ has attracted a lot of attention due to the availability of light energy, making it more environmentally friendly and energy efficient. Many researchers have developed photo-electrocatalytic techniques using semiconductor materials to utilize solar energy (Humayun *et al.*, 2018). One of the semiconductor materials that has been widely developed is TiO₂ because it is relatively efficient, inexpensive, inert, non-toxic, and has good photocatalytic activity (Hoang *et al.*, 2021). However, the use of TiO₂ with relatively large band gap energy (3.0 eV for the rutile phase and 3.2 eV for the anatase phase) requires ultraviolet (UV) light for electron-hole separation, so TiO₂ is not efficient in sunlight, which only contains ~5% UV light (Moghni *et al.*, 2022). Therefore, it is very important to develop photocatalysts that can be used in both visible light (400-700 nm) and ultraviolet (UV) light (290-400 nm) to increase photo-electrocatalytic efficiency.

* Corresponding author
Email: jarnuzi@ui.ac.id (J. Gunlazuardi)

Several modifications that can be made to increase the photo-electrocatalytic activity of TiO₂ in visible light are doping with metal and non-metallic elements, deposition with noble metals, combining other semiconductor materials to form heterojunctions and surface modification with inorganic acids (Zhang *et al.*, 2016). On the other hand, bismuth-based semiconductor materials have been widely developed for fixing nitrogen into ammonia because they show good activity as photocatalysts (Huang *et al.*, 2021). Shiraishi *et al.* (2020) developed a bismuth oxyhalide semiconductor [BiOX (X = Cl, Br, I)] with the consideration that BiOX is a non-toxic, inexpensive, and environmentally friendly semiconductor (Shiraishi *et al.*, 2020). On the other hand, TiO₂ has a high conduction band, so a semiconductor with an appropriate conduction band position is required. BiOBr is a semiconductor that responds to visible light and has a more negative conduction band than TiO₂. The use of BiOBr has attracted attention in composites with TiO₂, as this facilitates the injection of electrons from the conduction band of BiOBr into TiO₂ and reduces the recombination of photoelectrons and holes. (Jia *et al.*, 2018).

In this research, a tandem system of Dye-Sensitized Solar Cell (DSSC) and photo-electrochemical (PEC) cell was developed for the conversion of nitrogen to ammonia, aiming to reduce electrical energy consumption. The PEC cell served as a reaction site, utilizing visible light for the conversion process, while the DSSC cell will provide a source of electrons. The cathode and anode in the PEC cell was made of BiOBr/TiO₂ nanotubes, synthesized using the SILAR method (Sreedev *et al.*, 2019). BiOBr served as the catalyst for the photo-electrocatalytic conversion of N₂ to NH₃ on the cathode, while on the photoanode, BiOBr facilitated the efficient oxidation of H₂O. The DSSC zone utilized N719/TiO₂ nanotubes as the photoanode, Pt/FTO as the cathode, and electrolyte I⁻/I₃⁻. This research aims to produce ammonia with good solar to ammonia efficiency using environmentally friendly methods with low energy consumption.

2. Materials and Methods

2.1 Materials

The Ti plate, acetone (C₃H₆O), ethanol p.a (C₂H₅OH), ethylene glycol (C₂H₆O), ammonium fluoride (NH₄F), bismuth nitrate pentahydrate (Bi(NO₃)₃·5H₂O), ammonium chloride (NH₄Cl), sodium sulfate (Na₂SO₄), trisodium citrate (Na₃C₆H₅O₇), sodium hypochlorite (NaOCl), sodium hydroxide (NaOH), sodium nitroprusside (SNP), sodium bromide (NaBr), FTO, dye N719, Nafion membrane 117, phenol 99% and deionized water were purchased commercially. All materials were obtained from Sigma-Aldrich, except for the titanium plate (99.6% purity) obtained from Baoji Jinsheng Metal Material Co. Ltd and deionized water from OneMed.

2.2 Methods

2.2.1 Preparation of TiO₂ nanotubes (TiO₂NTs)

The titanium plate (6 cm x 1.5 cm x 0.02 cm) was cleaned through a sonication process at room temperature in acetone, ethanol, and water for 15 minutes each, then dried in air. All anodization experiments were carried out in an electrochemical cell of two electrodes. A Ti plate and stainless steel were used as the anode and cathode, respectively. An ethylene glycol solution containing 2% H₂O and 0.3% NH₄F was used as the electrolyte. The distance between the two electrodes was set at

about 1.5 cm. The anodization process was performed for 60 minutes at a potential of 40 V. After the anodization process, the sample was rinsed with deionized water and dried in the open air, then calcined for 2 hours at 450°C with a temperature increase rate of 5°C/minute (Surahman *et al.*, 2015).

2.2.2 Preparation of BiOBr/TiO₂ nanotubes (BiOBr/TiO₂NTs)

BiOBr/TiO₂NTs were prepared by the SILAR (Successive Ionic Layer Adsorption and Reaction) method, where 5 mM Bi(NO₃)₃·5H₂O and 5 mM NaBr were dissolved in 100 mL of 0,1 M mannitol solution and deionized water, respectively. TiO₂NTs were first immersed in Bi-solution for 1 minute, followed by rinsing with deionized water, then immersed in Br-solution for 1 minute, followed by rinsing with deionized water again. These experiments were carried out in a 40°C water bath to produce a depositing of BiOBr onto TiO₂NTs (Ma *et al.*, 2021). The above-mentioned process is called one cycle of the SILAR process and was repeated 5, 10, and 10 times. This variation SILAR cycle was denoted as BiOBr/TiO₂NTs (5), BiOBr/TiO₂NTs (10), and BiOBr/TiO₂NTs (15), respectively.

2.2.3 Preparation of dye-sensitized solar cell (DSSC)

There are three main components in DSSC, and those are N719/TiO₂NTs, Pt/FTO, and I⁻/I₃⁻ that were used as photoanode, cathode, and electrolyte solution, respectively. For N719/TiO₂NTs preparation, TiO₂NTs was immersed in 300 μM N719 dye solution (ethanol solvent) for 24 hours. After 24 hours of immersion, the N719 sensitized TiO₂NTs plate was cleaned with ethanol and dried in the air. For Pt/FTO preparation, the FTO glass (4 x 1.5 cm) was cleaned by sonication in ethanol for 10 minutes. The conducting part of the FTO glass dripped slowly with 20 mM H₂PtCl₆ solution in ethanol, dried in the open air, and then heated at 380°C for 30 minutes (Neetu *et al.*, 2017). The I⁻/I₃⁻ electrolyte solution was prepared by dissolving 0.13 g of I₂ crystals in a mixed solvent of 5 mL ethylene glycol and 20 mL acetonitrile, then adding 0.18 g of KI continuing by stirring for 30 minutes (Gu *et al.*, 2017).

The arrangement of the DSSC cells followed a sandwich cell configuration, where electrolyte I⁻/I₃⁻ was dripped on the surface of the photoanode (N719/TiO₂NTs), then parafilm was placed as a separator between the photoanode and cathode to avoid short circuit current, and then closed with a cathode (Pt/FTO). The photovoltaic performance of the DSSC was investigated by current–voltage (J–V) measurement under 40 Watt Phillips tungsten lamp as the source of visible light. By doing this measurement, a graph of current vs. potential was obtained. As the material was in the form of a plate, the current density was determined by dividing the measured current by the surface area of the plate that was immersed in the electrolyte.

Furthermore, the filling factor (FF) and η (% efficiency of DSSC) were calculated using the following equation (Chougala *et al.*, 2017):

$$FF = \frac{V_{max} \times J_{max}}{V_{oc} \times J_{sc}} \quad (1)$$

$$\eta (\% \text{ efficiency}) = \frac{FF \times J_{sc} \times V_{oc}}{I_0} \times 100\% \quad (2)$$

Where J_{sc} = short circuit current density, J_{max} = maximum power point current density, V_{oc} = open circuit voltage, and V_{max} = maximum power point voltage.

2.2.4 Electrochemical cell measurement

The preparation of the photo-electrochemical cell was carried out using a 3-electrode system potentiostat. The working electrodes were TiO₂NTs, BiOBr/TiO₂NTs, and N719/TiO₂NTs, while the counter electrode was Pt and the reference electrode was Ag/AgCl. A 40 Watt Phillips tungsten lamp was used as the source of visible light.

Electrochemical measurement for TiO₂NTs and BiOBr/TiO₂NTs was carried out using 0.1 M Na₂SO₄ electrolyte, and N719/TiO₂NTs was carried out using 0.01 M KI electrolyte in acetylacetone. Measurements were conducted using two methods, those are Linear Sweep Voltammetry (LSV) with a scan rate of 25 mV/s and Multi Pulsed Amperometry (MPA) with a constant potential of 0 V in dark and light conditions.

2.2.5 Preparation of the tandemsystem of DSSC-PEC for the conversion of nitrogen to ammonia

The conversion of nitrogen to ammonia was carried out in an H-type reactor connected with a Nafion membrane. BiOBr/TiO₂NTs served as the photoanode in the PEC cell for the water oxidation reaction to produce proton and electron. This electron will flow to the DSSC cathode (Pt/FTO). Meanwhile, the DSSC photoanode (N719/TiO₂NTs) acted as a source of electrons to the PEC cathode, where the reduction reaction of nitrogen to ammonia takes place, using BiOBr/TiO₂NTs as well. The PEC photoanode and DSSC cathode, as well as the DSSC photoanode and PEC cathode, were connected with Cu wires to facilitate the electron flow, as illustrated in Figure 1. Philips 400 Watt Tungsten lamp was used as a source of visible light radiation. The electrolyte used in the reactor was 0.1 M Na₂SO₄ solution with a reaction time of 6 hours. The NH₃ gas formed was absorbed in a 0.01 M HCl solution to form NH₄⁺ and then analyzed using spectrophotometric methods through phenate methods.

Ammonia levels were determined using the phenate method with a UV-Visible spectrophotometer at a wavelength of 640 nm which refers to SNI 06-6989.30-2005. Samples containing ammonia will form a blue indophenol complex when reacted with phenol, alkaline citrate solution (trisodium citrate, NaOH, and NaOCl), and sodium nitroprusside. A total of 5 mL

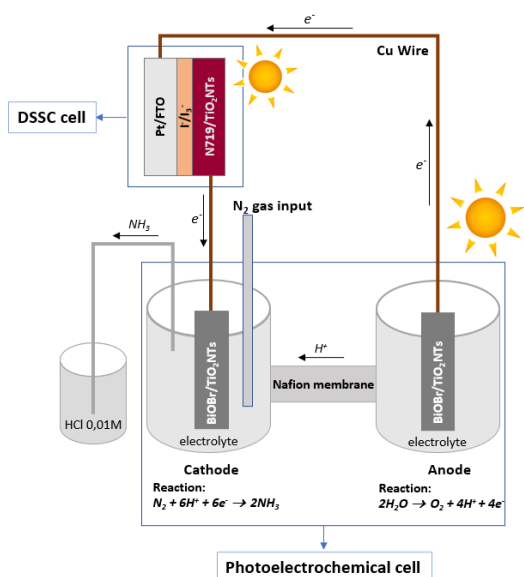


Fig. 1 The schematic diagram of the DSSC-PEC cell for conversion of nitrogen to ammonia

of sample or standard solution of NH₄Cl at various concentrations was added 0.2 mL of phenol solution; 0.2 mL nitroprusside; and 0.5 mL of oxidizing reagent (alkaline citrate solution), then homogenized and stored in a dark place for 2 hours. Then a blue color was formed and measured using a UV-Visible spectrophotometer at a wavelength of 640 nm.

Furthermore, the percent efficiency of conversion to ammonia was calculated using the Solar to Chemical Conversion (SCC) equation as follows (Shiraishi *et al.*, 2018):

$$SCC \text{ Efficiency (\%)} = \frac{[\Delta G \text{ for } NH_3 \text{ formation (Jmol}^{-1})] \times [NH_3 \text{ formed (mol)}]}{[\text{total input energy (W)}] \times [\text{reaction time (s)}]} \times 100\% \quad (3)$$

Where ΔG is the free energy of ammonia formation from nitrogen gas and water, which is 399 kJ/mol.

2.3 Characterization

TiO₂NTs and BiOBr/TiO₂NTs were characterized using XRD (X'pert PRO merk PANalytical MPD PAW3040/60), FTIR (Shimadzu IR Prestige 21), Raman Microscopes (HORIBA - The LabRAM HR Evolution), UV-Vis DRS (Shimadzu UV-2450), SEM-EDX (Quanta 650 of Thermo Scientific), and Potentiostat (PAR-VersaStat II). While N719/TiO₂NTs was characterized using FTIR, UV-Vis DRS, and Potentiostat.

Characterization of XRD was used to determine the crystallite size of the synthesized material. The crystallite size was estimated using the FWHM (full width at half maximum) of the high intensity peak appearing at $2\theta = 25.31^\circ$ (101) using the Scherer formula (Alkorbi *et al.*, 2022):

$$D = \frac{k\lambda}{\beta \cos\theta} \quad (4)$$

where D is the crystallite size (nm), k is a constant with the value of 0.89, λ is the X-ray wavelength (nm), θ is the Bragg angle (radians), and β is the FWHM (radians).

Meanwhile, the characterization using UV-Vis DRS was used to determine the energy band gap value. The energy band gap was determined by using the diffuse reflectance spectra and the Kubelka-Munk method according to the following equation (Garzon-Roman *et al.*, 2020),

$$F(R) = \frac{(1 - R)^2}{2R} \quad (5)$$

where R is the diffuse reflectance. In this case, F(R) becomes an absorbance function, and the following equation was used to determine the bandgap:

$$(F(R)hv)^{\frac{1}{2}} \text{ vs } E \quad (6)$$

3. Results and Discussion

3.1 Anodic oxidation of TiO₂NTs

Figure 2 shows the three stages of the formation of TiO₂NTs, the first stage (I) shows a very sharp decrease in current density from 22.2 mA/cm² to 4.48 mA/cm² in 50 seconds. The decrease in current is due to the oxidation of the Ti metal surface by releasing Ti⁴⁺ ions and electrons, which causes the formation of a TiO₂ oxide layer on the Ti metal surface. In this case, there was an interaction between water and oxidized Ti metal (Broens *et al.*, 2023). The TiO₂ oxide layer that was formed electrochemically acts as a barrier layer and obstructs the flow

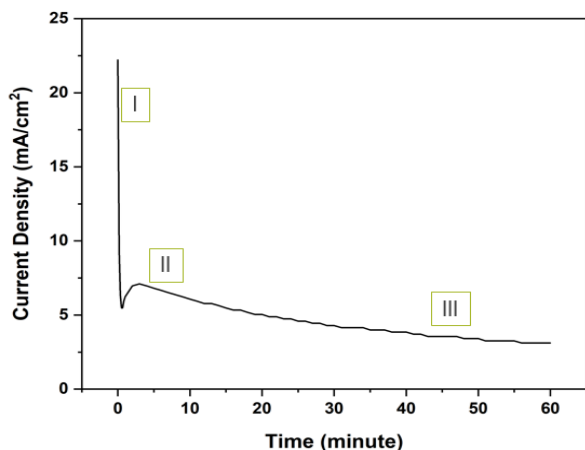
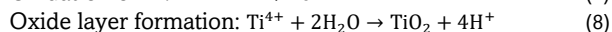
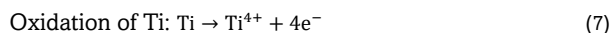
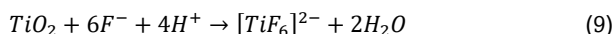


Fig. 2 Current density profile of TiO₂NTs formations

of ions and electrons so that the potential between titanium metal and the electrolyte decreases, which is indicated by a decrease in current during the anodization process (Qian *et al.*, 2022). According to (Indira *et al.*, 2015), the reactions that occur in the first stage (stage I) are as follows:



In stage II, the current increased from 4.48 mA/cm² to 7.11 mA/cm² within 40 seconds. The increase in current was caused by forming small holes and pores in the TiO₂ oxide layer through electric field dissolution reactions and chemical dissolution so that the anode was more conductive (Qin *et al.*, 2021). Small holes in the oxide layer were formed due to an electric field breaking the Ti and O bonds. The oxide layer with pinholes reacted with F⁻ (fluoride) ions and caused the current density to increase, as seen in stage II. This stage produced a porous oxide layer with a particular size and depth. The reaction of F⁻ ions with the oxide layer produced a complex compound [TiF₆]²⁻ with the following reaction (Indira *et al.*, 2015):



In stage III, there was a relatively stable decrease in current density. As the anodization time increased, the current decreased slightly due to the change in the pore depth of the holes formed. The pore growth rate and nanotube length were determined by the competition between electrochemical oxide formation and chemical dissolution by fluoride ions (Yoo *et al.*, 2018). This process produced a structure of vertically growing nanotubes. The TiO₂ material formed from the anodization process was amorphous. Next, a calcination process was carried out at 450°C for 2 hours to change from the amorphous phase to the anatase phase (Fang *et al.*, 2011).

3.2 XRD Patterns, structure, and morphology observations

Figure 3 shows the diffractogram of TiO₂NTs and BiOBr/TiO₂NTs. The 2θ value of the synthesized material was compared with the ICDD database. Based on ICDD data No. 01-089-4921 the typical peak of anatase TiO₂ is at position 25.36°; 37.85°; 48.15°; 53.97°; 55.19°; 62.81°; 68.88°; 74.18°; 75.21°; 76.22°. Based on ICDD data No. 00-044-1294 the typical peak of Ti metal is at position 35.09°; 38.42°; 40.17°; 53.01°; 70.66°; 82.29°; 86.76°; 92.73°. The typical peak produced by the synthesized material shows the peak according to the ICDD data. So, it can be known that the crystalline phase formed on the synthesized TiO₂NTs is the anatase phase. The estimated

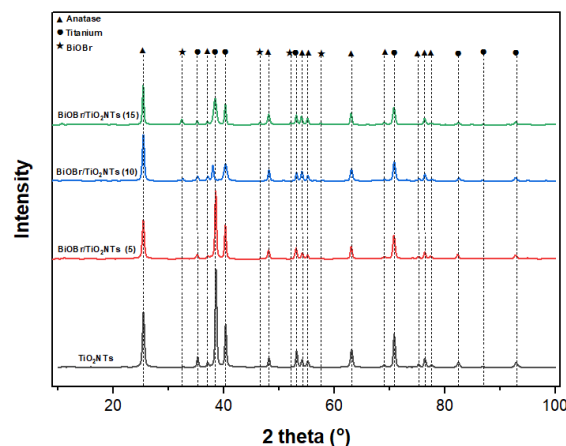


Fig. 3 XRD patterns of TiO₂NTs and BiOBr/TiO₂NTs

crystallite size of TiO₂NTs calculated using equation (4) was 26.23 nm.

In the BiOBr/TiO₂NTs diffraction pattern, several additional peaks were observed compared to the TiO₂NTs diffraction pattern. Based on ICDD data with reference code 00-003-0733, there are additional peaks at positions 2θ of 32.41°, 46.53°, 53.55°, and 57.56° respectively, according to the crystal plane (1 1 0), (2 0 0), (2 1 1), and (2 1 2) in the tetragonal phase of BiOBr (Yu *et al.*, 2023). As the SILAR cycle increased, the peak observed at position 2θ became clearer. In this case, the 15-cycle treatment showed a peak of 2θ for BiOBr, which was clearer than the 5 and 10-cycle treatments. This is because the more cycle variations, the more BiOBr will be deposited on the surface of TiO₂NTs so that more dominant BiOBr facets will be formed compared to fewer cycles.

Figure 4 shows the FTIR spectra of TiO₂NTs and BiOBr/TiO₂NTs to analyze functional groups. Based on the FTIR spectra, there were five main absorptions in BiOBr/TiO₂NTs. Ti-O stretching vibrations could be shown at 455-861 cm⁻¹, Ti-O-Ti stretching vibrations at 1630 cm⁻¹ (Singh & Dutta, 2018), OH bending vibrations at 1437-1600 cm⁻¹, OH stretching vibrations at 3000-3612 cm⁻¹, and Bi-O stretching vibration at 512 cm⁻¹ (Mera *et al.*, 2018).

Figure 5 shows the Raman spectra of BiOBr/TiO₂NTs compared to TiO₂NTs. It could be observed that there are several peaks which are typical peaks of anatase TiO₂ at Raman shifts of 147, 197, 395, 517, and 637 cm⁻¹ which correspond respectively to E_{g(1)}, E_{g(2)}, B_{1g}, A_{1g} and E_{g(3)} for the anatase phase mode. The E_g mode could appear due to the O-Ti-O

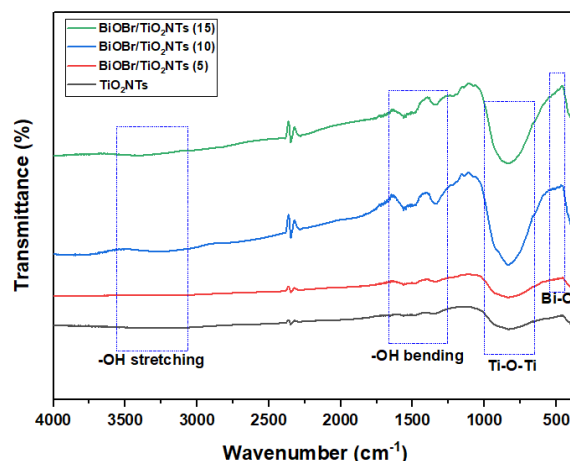


Fig. 4 FTIR spectra of TiO₂NTs and BiOBr/TiO₂NTs

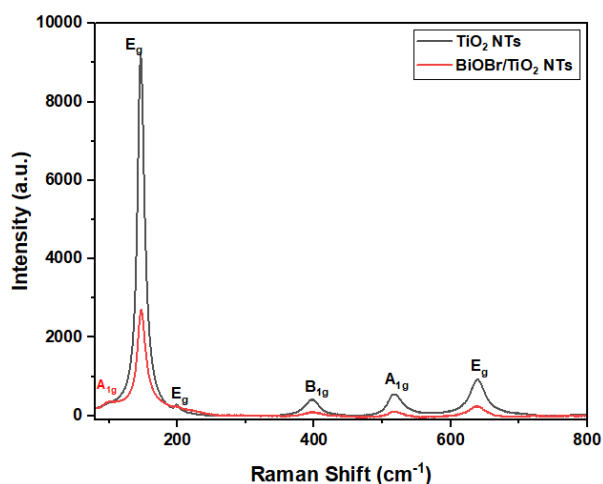


Fig. 5 Raman spectra of TiO_2NTs and $\text{BiOBr}/\text{TiO}_2\text{NTs}$

symmetrical stretching vibration, the B_{1g} mode was assigned to the O–Ti–O symmetric bending vibration, and the A_{1g} mode corresponded to the Ti–O–Ti antisymmetric bending vibration in TiO_2 . These results were consistent with research conducted by (Boda & Shah, 2017) which showed that the Raman spectra of TiO_2NTs could be observed in the range of $245 - 351\text{cm}^{-1}$ which corresponds to the covalent interaction of O–O. The active mode at 147 and 197cm^{-1} were assigned to the unit cell's Ti interaction. The strongest mode that appears at 147cm^{-1} is due to external symmetrical vibrations confirming the anatase phase's formation. In addition, there was an additional peak at 125cm^{-1} which corresponds to the A_{1g} stretching vibration of the Bi–Br bond. Based on the literature (Wang *et al.*, 2016), three characteristic bands in BiOBr could be observed at 112 , 162 , and 385cm^{-1} which correspond respectively to the A_{1g} internal stretching vibration of the Bi–Br bond, the E_g internal stretching vibration of the Bi–Br bond and the B_{1g} band generated by the vibration oxygen atom from the Bi–O bond. However, in the results of this study, only the A_{1g} band could be clearly observed in the Raman spectra of $\text{BiOBr}/\text{TiO}_2\text{NTs}$, while the two characteristic bands could not be observed clearly. This might

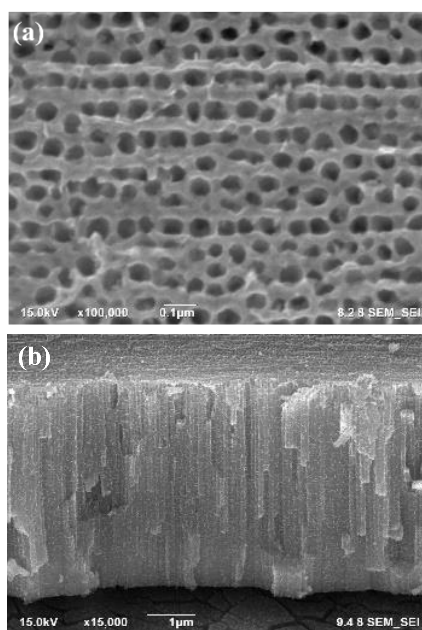


Fig. 6 SEM images of $\text{BiOBr}/\text{TiO}_2\text{NTs}$ 15 SILAR cycles (a) surface with $100,000\times$ magnification and (b) cross section with $15,000\times$ magnification

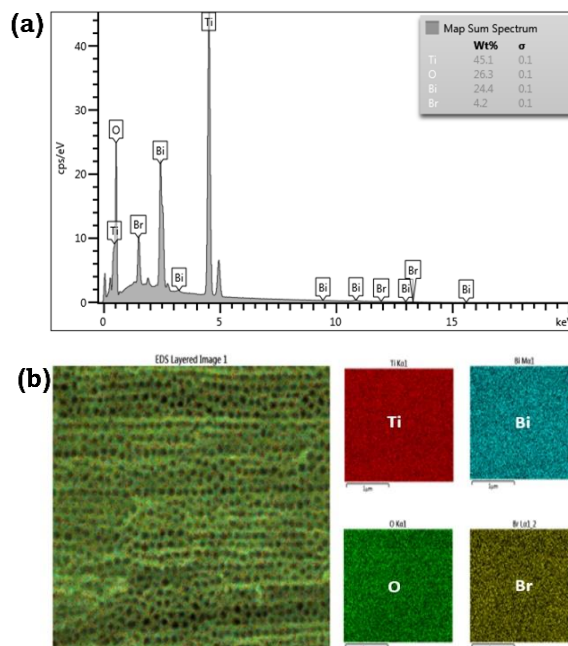


Fig. 7 EDX point (a) and mapping (b) of $\text{BiOBr}/\text{TiO}_2\text{NTs}$

be caused by the two other bands overlapping with the characteristic Raman band of TiO_2NTs , whose intensity was very strong so that the characteristic band of $\text{BiOBr}/\text{TiO}_2\text{NTs}$ could not be observed clearly.

SEM images of $\text{BiOBr}/\text{TiO}_2\text{NTs}$ (Figure 6a) show the morphology of the surface of $\text{BiOBr}/\text{TiO}_2\text{NTs}$ (15) at $100,000\times$ magnification. Based on these results, it could be observed that TiO_2 was formed with nanotube morphology deposited by BiOBr on the surface, which is marked by a white color on the surface of TiO_2NTs , and the tube of TiO_2NTs was still visible. This result shows that the deposition of BiOBr on the surface of TiO_2NTs did not block the mouth of the tube. Figure 6(b) shows the morphology of the $\text{BiOBr}/\text{TiO}_2\text{NTs}$ cross-section with a magnification of $15,000$ times showing a tube height of $4.4\ \mu\text{m}$ and it could be observed that the cross section showed several small particles indicating the BiOBr compound.

In addition to characterization using SEM, characterization was also carried out using EDX which aims to determine the composition of each constituent element. Figure 7(a) shows the point EDX spectra of $\text{BiOBr}/\text{TiO}_2\text{NTs}$ (15). These results indicated the presence of Bi and Br elements, in addition to Ti and O from TiO_2 compounds which allows the formation of BiOBr on the surface of TiO_2 . Figure 7(b) shows the EDX mapping of $\text{BiOBr}/\text{TiO}_2\text{NTs}$ (15) indicating that the elements Bi, O, Br, and Ti have been formed and distributed evenly.

3.3 Optical absorption and photo-electrochemical performance

Figure 8 shows the results of the characterization using UV-DRS. The more SILAR cycles indicate a shift in the wavelength absorption toward the visible region. For $\text{BiOBr}/\text{TiO}_2\text{NTs}$ (15), $\text{BiOBr}/\text{TiO}_2\text{NTs}$ (10), and $\text{BiOBr}/\text{TiO}_2\text{NTs}$ (5) the UV-Vis diffuse reflectance spectroscopy (DRS) spectra present a slight red shift of adsorption edge and a higher visible light absorbance. The Kubelka-Munk model, presented in equation (5), was used to estimate the band gap energy of all samples by plotting $(F(R)h\nu)^{1/2}$ versus the energy of absorbed light (Landi *et al.*, 2022). The band gap energy values obtained for TiO_2NTs

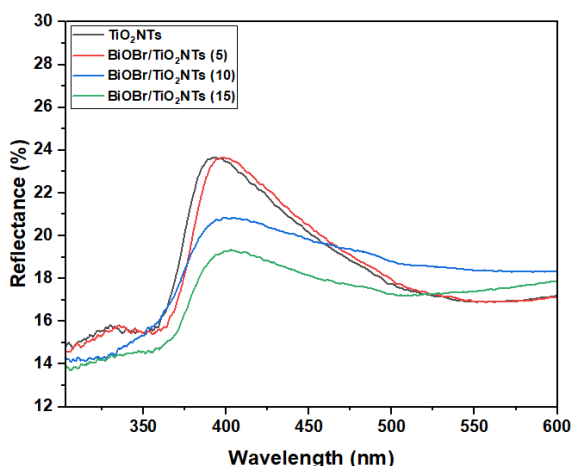


Fig. 8 UV-DRS spectra of TiO₂NTs and BiOBr/TiO₂NTs

was 3,20 eV, and for each variation of BiOBr/TiO₂NTs, were 2.96 eV, 2.94 eV, and 2.92 eV, respectively for 5x, 10x, and 15x cycles of SILAR process. These results indicated that the more SILAR cycles, the more BiOBr would be deposited on the TiO₂NTs surface, making it more active under visible light. This was indicated by shifting the absorption to the visible region and the decrease in the band gap energy, which becomes smaller.

Figure 9 shows electrochemical performance results using the LSV and MPA methods. Under visible light irradiation, measurements using the LSV method were carried out over a potential range of -1V to +1V. These results indicated that the deposition of BiOBr on the surface of TiO₂NTs could increase the resulting current density compared to TiO₂NTs without

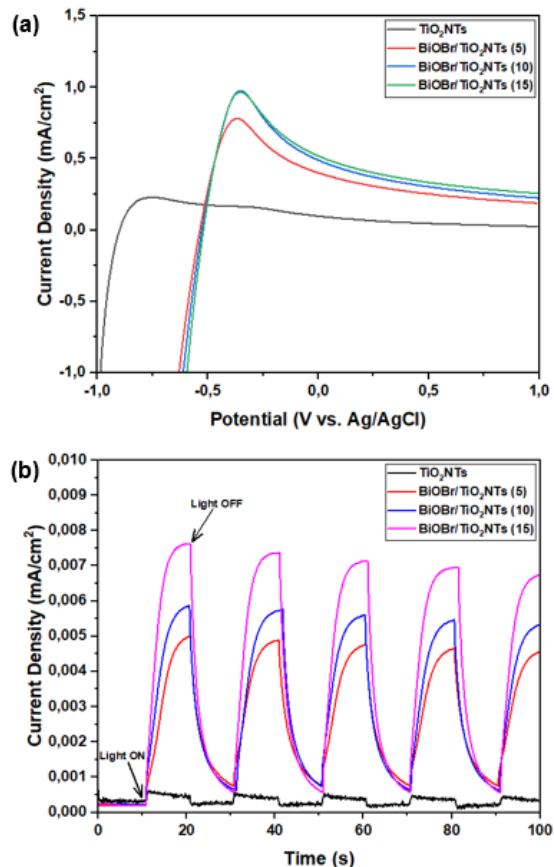


Fig. 9 Electrochemical Performance of TiO₂NTs and BiOBr/TiO₂NTs using (a) Linear Sweep Voltammetry (LSV) method and (b) Multi Pulse Amperometry (MPA) method under visible light irradiation

adding BiOBr (Figure 9a). The highest current density was produced in BiOBr/TiO₂NTs (15), with a variation of 15x SILAR cycles, because more BiOBr might be deposited on the surface of TiO₂NTs. As a result, the current density was higher in irradiation using visible lamps compared to 5 and 10 cycles. Figure 9(b) shows the measurement results using the MPA method on BiOBr/TiO₂NTs within 100 seconds in dark and light conditions alternately with a duration of 10 seconds for each condition. These results indicated that when the BiOBr/TiO₂NTs were irradiated using a visible lamp, there was an increase in current density, and when the visible light was turned off, there was a significant decrease in current density. The results of this measurement indicated that BiOBr/TiO₂NTs had a higher current density response when compared to TiO₂NTs, where BiOBr/TiO₂NTs produced the highest current density with 15 SILAR cycles.

Based on measurements using the LSV and MPA methods, it shows that the deposition of BiOBr on the surface of TiO₂NTs could increase the current density, which makes it active in the visible region, compared to TiO₂NTs without modification with BiOBr. This result was observed because the addition of BiOBr could produce oxygen vacancies on the surface, increasing photocatalytic activity and exhibiting higher intensity of photocurrent. It suggests that the photo-induced hole-electron pairs in BiOBr are efficiently separated (Wang *et al.*, 2021).

3.4 DSSC efficiency

The DSSC components were arranged like a sandwich structure using N719/TiO₂NTs as the anode, Pt/FTO as the cathode, and I⁻/I₃⁻ as the electrolyte solution. In addition, a parafilm spacer was used as a barrier between the anode and cathode to avoid short circuits. DSSC performance was carried out using a potentiostat by connecting the anode and reference wires to the N719/TiO₂NTs plate and the cathode wires to the Pt/FTO. Figure 10 shows the photocurrent-to-potential curve given the irradiation conditions using a visible lamp. Efficiency was determined based on data from the photocurrent-to-potential change curve. Based on this curve, several parameters were obtained that could be used to calculate the filling factor and DSSC efficiency, and those are short circuit current density (J_{sc}), maximum power point current density (J_{max}), open circuit voltage (V_{oc}), maximum power point voltage (V_{max}) with the resulting values respectively 0.2028 mA/cm², 0.1202 mA/cm², 0.5280 V, and 0.320 V.

Based on the results of the calculation using equation (1) and (2), by using the total incident irradiance (I₀) of 2.58 mW/cm²,

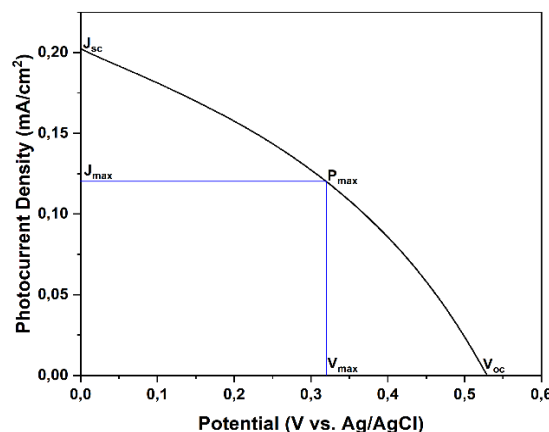


Fig. 10 Photocurrent density vs. potential of DSSC

Table 1

The amount of ammonia produced

Irradiation time (hour)	Concentration (ppm)	Amount of ammonia (μmol)	SCC (%)
2	0.0947	0.0557	0.0028
4	0.1393	0.0819	0.0021
6	0.2162	0.1272	0.0021

the FF value is 0.3592, and the DSSC efficiency is 1.49%. This DSSC cell will be used in a DSSC-PEC tandem system for the conversion of nitrogen to ammonia to increase the electrons that would be entering the catalysis zone so that more ammonia will be produced.

3.5 Conversion of nitrogen to ammonia in a DSSC-PEC tandem system

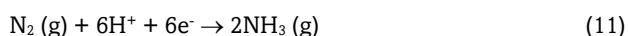
The conversion of nitrogen to ammonia was carried out in an H-type reactor that utilizes the DSSC-PEC system. The conversion reaction of nitrogen was a reduction reaction that occurs at the PEC cathode. The PEC cathode was connected to N719/TiO₂NTs, which functions as a DSSC anode for visible light harvesting. Meanwhile, the PEC anode was where the water oxidation reaction occurs, producing electrons (e⁻) and protons (H⁺). These electrons would go to the DSSC cathode (Pt/FTO) through an external circuit which would later be used to reduce I₃⁻ to I⁻ ions in DSSC. At the same time, the protons would go to the PEC cathode through the Nafion membrane, which would involve converting nitrogen into ammonia.

In the photoanode part of the PEC cell, BiOBr/TiO₂NTs (15) were used, which is expected to facilitate the oxidation reaction of water into electrons (e⁻) and protons (H⁺) under visible light radiation. While at the PEC cathode, BiOBr/TiO₂NTs (15) were used to facilitate the conversion process of nitrogen to ammonia through the reduction reaction. The reaction is as follows:

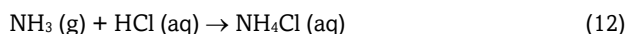
Reaction at the photoanode:



Reaction at the cathode:



Furthermore, the resulting ammonia flowed into a glass containing 0.01 M HCl solution to produce ammonium chloride solution with the following reaction:



The experiment was carried out for 6 hours, where samples were taken every 2 hours. The samples were analyzed spectrophotometrically using the phenate method. Table 1 shows the amount of ammonia produced within 2, 4, and 6 hours. This data shows that the longer the irradiation time, the more ammonia will be produced. When irradiated by visible light in the anode, holes transferred from TiO₂ to BiOBr for the oxidation reaction of water, while in the cathode, electrons on BiOBr transferred to the TiO₂ surface for nitrogen fixation reaction. The photo-electrocatalytic activity of BiOBr/TiO₂NTs heterojunction could be ascribed to effective interfacial interaction (Wang *et al.*, 2021).

Furthermore, the percent efficiency of conversion to ammonia was calculated using equation (3). The total energy input (W) is the amount of light given from the irradiation source to the active area of the DSSC. The light intensity used in this

study was 312.5 W/m² with an irradiated DSSC area of 0.0003 m², so the total power input generated was 0.09375 Watts. Based on the calculations, the Solar to Chemical Conversion (SCC) percentage was 0.0028%, 0.0021%, and 0.0021% for a reaction time of 2, 4, and 6 hours, respectively.

In comparison to Hirakawa *et al.*'s research (2017), where the SCC was reported to be 0.02%, our result is lower. This discrepancy may be due to the fact that they used TiO₂ in powder form, which increased the contact area between the catalyst and the reactants. They also used a higher lamp power, which excited more electrons from the valence band to the conduction band (Hirakawa *et al.*, 2017). However, our results are consistent with An'Nur *et al.*'s (2020) research, where the SCC value for ammonia production using a DSSC-PEC system was reported to be 0.005% after 24 hours of irradiation (An'Nur *et al.*, 2020). It should be noted that the difference in SCC values between our study and An'Nur *et al.*'s study may also be attributed to the difference in the duration of the experiment. While our study was conducted for 6 hours, An'Nur *et al.* carried out their experiment for 24 hours. The longer duration of their experiment might have allowed for more ammonia production, leading to a higher SCC value. However, despite the shorter duration of our experiment, our study still provides valuable insights into the potential use of DSSC-PEC systems for solar-driven ammonia synthesis.

4. Conclusion

In summary, we have developed the combined system of DSSC-PEC to convert nitrogen to ammonia under visible light without external input energy. BiOBr/TiO₂NTs heterojunction in the PEC cell was obtained through a facile synthesis using the SILAR method. The characterization showed that BiOBr was well deposited on the surface of the TiO₂ nanotubes to form the desired heterojunction structure. In the DSSC cell, N719/TiO₂NTs-based material converted light energy to produce active electrons to be injected into the PEC cathode for nitrogen reduction. The ammonia produced was 0.1272 μmol for 6 hours, with the percentage of SCC being 0.0021%. This work provides new prospects for developing the construction of the combined system of DSSC-PEC using heterojunction catalysts for efficient photo-electrocatalytic nitrogen conversion to ammonia.

Acknowledgments

The authors would like to thank the Ministry of Education, Culture, Research, and Technology, which has provided research funding through Penelitian Tesis Magister (PTM) in 2022.

Author Contributions: P.A.: performed the experiments and data analysis, methodology, writing—original draft, review and editing. J.G.: supervision, project administration, writing—review and editing.

validation. All authors have read and agreed to the published version of the manuscript.

Funding: This research was funded by the Ministry of Education, Culture, Research, and Technology, Contract Number 987/UN2.RST/HKP.05.00/2022.

Conflicts of Interest: The authors declare no conflict of interest.

References

- Alkorbi, A. S., Muhammad Asif Javed, H., Hussain, S., Latif, S., Mahr, M. S., Mustafa, M. S., Alsaiani, R., & Alhemiary, N. A. (2022). Solar light-driven photocatalytic degradation of methyl blue by carbon-doped TiO₂ nanoparticles. *Optical Materials*, 127, 112259. <https://doi.org/10.1016/j.optmat.2022.112259>
- An'Nur, F. K., Wihelmina, B. V., Gunlazuardi, J., & Wibowo, R. (2020). Tandem system of dyes sensitized solar cell-photo electro chemical (DSSC-PEC) employing TiO₂ nanotube/BiOBr as dark cathode for nitrogen fixation. *AIP Conference Proceedings*, 2243(June 2020). <https://doi.org/10.1063/5.0001100>
- Boda, M. A., & Shah, M. A. (2017). Fabrication mechanism of compact TiO₂ nanotubes and their photo-electrochemical ability. *Materials Research Express*, 4(7). <https://doi.org/10.1088/2053-1591/aa7cd2>
- Broens, M. I., Ramos Cervantes, W., Asenjo Collao, A. M., Iglesias, R. A., Teijelo, M. L., & Linarez Pérez, O. E. (2023). TiO₂ nanotube arrays grown in ethylene glycol-based media containing fluoride: Understanding the effect of early anodization stages on the morphology. *Journal of Electroanalytical Chemistry*, 935, 117314. <https://doi.org/10.1016/j.jelechem.2023.117314>
- Chougala, L. S., Yatnatti, M. S., Lingangoudar, R. K., Kamble, R. R., & Kadadevarmath, J. S. (2017). A simple approach on synthesis of TiO₂ nanoparticles and its application in dye sensitized solar cells. *Journal of Nano- and Electronic Physics*, 9(4). [https://doi.org/10.21272/jnep.9\(4\).04005](https://doi.org/10.21272/jnep.9(4).04005)
- Fang, D., Luo, Z., Huang, K., & Lagoudas, D. C. (2011). Effect of heat treatment on morphology, crystalline structure and photocatalysis properties of TiO₂ nanotubes on Ti substrate and freestanding membrane. *Applied Surface Science*, 257(15), 6451–6461. <https://doi.org/10.1016/j.apsusc.2011.02.037>
- Feng, J., Zhang, X., Zhang, G., Li, J., Song, W., & Xu, Z. (2021). Improved photocatalytic conversion of high-concentration ammonia in water by low-cost Cu/TiO₂ and its mechanism study. *Chemosphere*, 274. <https://doi.org/10.1016/j.chemosphere.2021.129689>
- Garzon-Roman, A., Zuñiga-Islas, C., & Quiroga-González, E. (2020). Immobilization of doped TiO₂ nanostructures with Cu or In inside of macroporous silicon using the solvothermal method: Morphological, structural, optical and functional properties. *Ceramics International*, 46(1), 1137–1147. <https://doi.org/10.1016/j.ceramint.2019.09.082>
- Gu, P., Yang, D., Zhu, X., Sun, H., Wangyang, P., Li, J., & Tian, H. (2017). Influence of electrolyte proportion on the performance of dye-sensitized solar cells. *AIP Advances*, 7(10). <https://doi.org/10.1063/1.5000564>
- Hirakawa, H., Hashimoto, M., Shiraishi, Y., & Hirai, T. (2017). Photocatalytic Conversion of Nitrogen to Ammonia with Water on Surface Oxygen Vacancies of Titanium Dioxide. *Journal of the American Chemical Society*, 139(31), 10929–10936. <https://doi.org/10.1021/jacs.7b06634>
- Hoang, N. T.-T., Tran, A. T.-K., Le, T.-A., & Nguyen, D. D. (2021). Enhancing efficiency and photocatalytic activity of TiO₂-SiO₂ by combination of glycerol for MO degradation in continuous reactor under solar irradiation. *Journal of Environmental Chemical Engineering*, 9(5), 105789. <https://doi.org/10.1016/j.jece.2021.105789>
- Huang, R., Li, X., Gao, W., Zhang, X., Liang, S., & Luo, M. (2021). Recent advances in photocatalytic nitrogen fixation: From active sites to ammonia quantification methods. *RSC Advances*, 11(24), 14844–14861. <https://doi.org/10.1039/d0ra10439f>
- Humayun, M., Raziq, F., Khan, A., & Luo, W. (2018). Modification strategies of TiO₂ for potential applications in photocatalysis: A critical review. *Green Chemistry Letters and Reviews*, 11(2), 86–102. <https://doi.org/10.1080/17518253.2018.1440324>
- Indira, K., Mudali, U. K., Nishimura, T., & Rajendran, N. (2015). A Review on TiO₂ Nanotubes: Influence of Anodization Parameters, Formation Mechanism, Properties, Corrosion Behavior, and Biomedical Applications. *Journal of Bio- and Tribo-Corrosion*, 1(4), 1–22. <https://doi.org/10.1007/s40735-015-0024-x>
- Jia, L., Tan, X., Yu, T., & Zhang, Z. (2018). Enhanced photoelectrocatalytic performance of temperature-dependent 2D/1D BiOBr/TiO₂-x nanotubes. *Materials Research Bulletin*, 105, 322–329. <https://doi.org/10.1016/j.materresbull.2018.05.005>
- Lan, M., Zheng, N., Dong, X., Ma, H., & Zhang, X. (2021). One-step in-situ synthesis of Bi-decorated BiOBr microspheres with abundant oxygen vacancies for enhanced photocatalytic nitrogen fixation properties. *Colloids and Surfaces A: Physicochemical and Engineering Aspects*, 623, 126744. <https://doi.org/10.1016/j.colsurfa.2021.126744>
- Landi, S., Segundo, I. R., Afonso, C., Lima, O., Costa, M. F. M., Freitas, E., & Carneiro, J. (2022). Evaluation of band gap energy of TiO₂ precipitated from titanium sulphate. *Physica B: Condensed Matter*, 639, 10–13. <https://doi.org/10.1016/j.physb.2022.414008>
- Li, H., Shang, J., Ai, Z., & Zhang, L. (2015). Efficient visible light nitrogen fixation with BiOBr nanosheets of oxygen vacancies on the exposed {001} Facets. *Journal of the American Chemical Society*, 137(19), 6393–6399. <https://doi.org/10.1021/jacs.5b03105>
- Ma, B., Xin, S., Xin, Y., Ma, X., Zhang, C., & Gao, M. (2021). Optimized fabrication of BiOBr/TiO₂ nanotube arrays for efficient degradation of organic pollutant under visible light irradiation. *Journal of Environmental Chemical Engineering*, 9(2), 104833. <https://doi.org/10.1016/j.jece.2020.104833>
- Mera, A. C., Rodríguez, C. A., Valdés, H., Jaramillo, A. F., Rojas, D., & Meléndrez, M. F. (2018). Solvothermal synthesis and photocatalytic activity of BiOBr microspheres with hierarchical morphologies. *Acta Chimica Slovenica*, 65(2), 429–437. <https://doi.org/10.17344/acsi.2018.4181>
- Moghni, N., Boutoumi, H., Khalaf, H., Makaoui, N., & Colón, G. (2022). Enhanced photocatalytic activity of TiO₂/WO₃ nanocomposite from sonochemical-microwave assisted synthesis for the photodegradation of ciprofloxacin and oxytetracycline antibiotics under UV and sunlight. *Journal of Photochemistry and Photobiology A: Chemistry*, 428(February), 448. <https://doi.org/10.1016/j.jphotochem.2022.113848>
- Neetu, Maurya, I. C., Singh, S., Gupta, A. K., Srivastava, P., & Bahadur, L. (2017). N/Al-Incorporated TiO₂ Nanocomposites for Improved Device Performance of a Dye-Sensitized Solar Cell. *ChemistrySelect*, 2(15), 4267–4276. <https://doi.org/10.1002/slct.201700550>
- Olabi, A. G., Abdelkareem, M. A., Al-Murisi, M., Shehata, N., Alami, A. H., Radwan, A., Wilberforce, T., Chae, K. J., & Sayed, E. T. (2023). Recent progress in Green Ammonia: Production, applications, assessment; barriers, and its role in achieving the sustainable development goals. *Energy Conversion and Management*, 277, 116594. <https://doi.org/10.1016/j.enconman.2022.116594>
- Qian, Q., Lin, Y., Xiong, Z., Su, P., Liao, D., Dai, Q., Chen, L., & Feng, D. (2022). Internal anodization of porous Ti to fabricate immobilized TiO₂ nanotubes with a high specific surface area. *Electrochemistry Communications*, 135, 107201. <https://doi.org/10.1016/j.elecom.2022.107201>
- Qin, J., Cao, Z., Li, H., & Su, Z. (2021). Formation of anodic TiO₂ nanotube arrays with ultra-small pore size. *Surface and Coatings Technology*, 405, 126661. <https://doi.org/10.1016/j.surfcoat.2020.126661>
- Shiraishi, Y., Hashimoto, M., Chishiro, K., Moriyama, K., Tanaka, S., & Hirai, T. (2020). Photocatalytic Dinitrogen Fixation with Water on Bismuth Oxychloride in Chloride Solutions for Solar-to-Chemical Energy Conversion. *Journal of the American Chemical Society*, 142(16), 7574–7583. <https://doi.org/10.1021/jacs.0c01683>
- Shiraishi, Y., Shiota, S., Kofuji, Y., Hashimoto, M., Chishiro, K., Hirakawa, H., Tanaka, S., Ichikawa, S., & Hirai, T. (2018). Nitrogen Fixation with Water on Carbon-Nitride-Based Metal-

- Free Photocatalysts with 0.1% Solar-to-Ammonia Energy Conversion Efficiency [Research-article]. *ACS Applied Energy Materials*, 1(8), 4169–4177. <https://doi.org/10.1021/acsaem.8b00829>
- Singh, R., & Dutta, S. (2018). Synthesis and characterization of solar photoactive TiO₂ nanoparticles with enhanced structural and optical properties. *Advanced Powder Technology*, 29(2), 211–219. <https://doi.org/10.1016/j.apt.2017.11.005>
- Sreedev, P., Rakhesh, V., Roshima, N. S., & Shankar, B. (2019). Preparation of Zinc Oxide Thin films by SILAR method and its Optical analysis. *Journal of Physics: Conference Series*, 1172(1). <https://doi.org/10.1088/1742-6596/1172/1/012024>
- Surahman, H., Krisnandi, Y. K., & Gunlazuardi, J. (2015). Modification of Mixed Structure TiO₂ Nanoporous- Nanotube Arrays with CdS Nanoparticle and Their Photoelectrochemical Properties. *Jurnal Sains Materi Indonesia*, 16(3), 118–125. <https://jurnal.batan.go.id/index.php/jsmi/article/view/4229>
- Wang, J., Fang, Y., Zhang, W., Yu, X., Wang, L., & Zhang, Y. (2021). TiO₂/BiOBr 2D-2D heterostructure via in-situ approach for enhanced visible-light photocatalytic N₂ fixation. *Applied Surface Science*, 567, 150623. <https://doi.org/10.1016/j.apsusc.2021.150623>
- Wang, L., Wang, S., Li, M., Yang, X., Li, F., Xu, L., & Zou, Y. (2022). Constructing oxygen vacancies and linker defects in MIL-125 @TiO₂ for efficient photocatalytic nitrogen fixation. *Journal of Alloys and Compounds*, 909, 164751. <https://doi.org/10.1016/j.jallcom.2022.164751>
- Wang, X. J., Zhao, Y., Li, F. T., Dou, L. J., Li, Y. P., Zhao, J., & Hao, Y. J. (2016). A Chelation Strategy for In-situ Constructing Surface Oxygen Vacancy on {001} Facets Exposed BiOBr Nanosheets. *Scientific Reports*, 6, 1–11. <https://doi.org/10.1038/srep24918>
- Yoo, H., Kim, M., Kim, Y. T., Lee, K., & Choi, J. (2018). Catalyst-doped anodic TiO₂ nanotubes: Binder-free electrodes for (photo)electrochemical reactions. *Catalysts*, 8(11), 1–25. <https://doi.org/10.3390/catal8110555>
- Yu, H., Li, J., Lin, Y., Wang, Z., Peng, H., Tao, H., Lai, X., & Huang, Y. (2023). BiOBr cluster spheres grown on conductive glass for a recyclable and efficient photocatalytic reactor. *Materials Letters*, 331, 133536. <https://doi.org/10.1016/j.matlet.2022.133536>
- Zhang, X., Yang, H., Zhang, B., Shen, Y., & Wang, M. (2016). BiOI-TiO₂ Nanocomposites for Photoelectrochemical Water Splitting. *Advanced Materials Interfaces*, 3(1), 3–7. <https://doi.org/10.1002/admi.201500273>



© 2023. The Author(s). This article is an open access article distributed under the terms and conditions of the Creative Commons Attribution-ShareAlike 4.0 (CC BY-SA) International License (<http://creativecommons.org/licenses/by-sa/4.0/>)